



Immobilization of gold on short-channel mesoporous SBA-15 functionalized with thiol and hydrophobic groups for oxidation reactions

R. de la Serna Valdés, J. Agúndez, C. Márquez-Álvarez, J. Pérez-Pariente*

Instituto de Catálisis y Petroleoquímica (ICP-CSIC), Marie Curie 2, 28049, Cantoblanco, Madrid, Spain

ARTICLE INFO

Keywords:

Short-channel SBA-15
Dimethyldioxirane
Gold clusters
Cyclohexene
Oxidation
Hydrophobicity

ABSTRACT

Nanosized gold entities immobilized on short-channel SBA-15 mesoporous materials functionalized solely with mercaptopropyl groups and together with propyl and octyl moieties have been prepared following a two-steps procedure. These materials have been used as catalysts for the oxidation of cyclohexene with molecular oxygen in liquid phase at atmospheric pressure. First, SBA-15 materials functionalized only with mercaptopropyl groups and with a combination of these groups with two hydrophobic moieties, namely propyl and octyl, have been synthesized in the presence of the non-ionic surfactant P104. Small particles having short channel length have been identified by TEM and SEM. In order to study the influence of the nature of the sulphur functional group, these S-bearing materials were also oxidized with hydrogen peroxide or dimethyldioxirane (DMD) to sulfonic groups prior to gold immobilization. The effectiveness of these oxidation methods was assessed by ^{29}Si MAS NMR, ^{13}C CP MAS NMR, XPS, chemical and thermal analysis, and it has been found that DMD oxidized efficiently thiol groups to sulfonic groups, but H_2O_2 leaves a fraction of unreacted thiol. In a second step, nanosized gold entities have been prepared by a two-liquid phases route involving rosemary oil as organic phase and an aqueous phase formed by dissolving gold in a solution of ammonium chloride in concentrated nitric acid (*aqua regia*). Following this method, a fraction of the Au dissolved in the *aqua regia* solution is spontaneously reduced and transferred to the essential oil phase. Upon contacting the gold-bearing organic layer with the mesoporous materials, gold is actually immobilized on them, rendering metal contents in the range 1.1–0.2 wt.%, being those functionalized with alkyl chains the least efficient in capturing gold from the organic phase. No surface plasmon resonance band at 520 nm characteristic of gold nanoparticles has been detected by UV–vis spectroscopy in these Au-containing materials. All of them are active and selective for the allylic oxidation of cyclohexene, but their specific activity varies as a function of the nature of the functional groups. It has been found that the most active catalysts are those pre-oxidized with DMD. The presence of hydrophobic octyl groups increases substantially the turnover number of the reaction (TON), while the short-chain propyl moieties hardly affect the activity. It has been found that the nanosized gold entities initially present in the catalysts evolve in the reaction medium towards the formation of nanoparticles.

1. Introduction

Chemical and catalytic reactivity of gold nanoparticles is affected by a variety of different factors, as their size and shape, and, if they are supported on a solid material, also by the specific characteristics of the support, as they can control not only the metal-support interaction, but also the diffusion and adsorption/desorption of reagents and products under actual reaction conditions [1–3]. It is possible in a first approach to gain some control on these properties by using specific synthesis procedures of both the gold entities and the support on which they would eventually be immobilized. On this regard, we have shown [4] that it is possible to prepare nanosized gold by using a two-liquid

phases system reported in mid eighteenth century scientific literature [5], involving the use of essential oils as organic phase and a solution of gold in a mixture of concentrated nitric acid and ammonium chloride (this a variety of *aqua regia*). In this system, a fraction of the gold is spontaneously reduced and transferred to the essential oil phase, which contains small disordered Au clusters of about 1–1.5 nm in size, together with Au nanoparticles (AuNPs) in the range of 2–20 nm, but 90% of them in the range of 2–8 nm [4]. Hence, this method predates by one century the most widely known two-liquid phases methodology reported by Michael Faraday in the nineteenth century [6,7]. Moreover, it has been found that the formation of nanoparticles can be suppressed by adjusting the gold concentration in the aqueous phase, and therefore

* Corresponding author.

E-mail address: jperez@icp.csic.es (J. Pérez-Pariente).

<https://doi.org/10.1016/j.cattod.2019.09.014>

Received 21 December 2018; Received in revised form 19 June 2019; Accepted 11 September 2019

0920-5861/ © 2019 Elsevier B.V. All rights reserved.

this is a suitable and simple method to obtain gold entities with size below ~ 2 nm [8].

Ordered mesoporous silica materials are very convenient supports for the immobilization of nanosized gold, owing to their tunable (within certain limits) porous structure, large pore size and surface area, and the possibility to decorate the surface with functional groups with the potential capability of interacting with deposited gold nanosized entities, rendering high dispersion and preventing them from agglomeration and leaching [9]. Moreover, it is well-known that gold has strong affinity for thiols [10,11]. For these reasons, the nanosized Au entities prepared by the essential oil-mediated route described above have been immobilized on mesoporous SBA-15 materials functionalized with propylthiol moieties as gold binding groups [8]. However, it has been found that the Au-thiol catalysts are inactive for the liquid phase oxidation of cyclohexene with molecular oxygen, and the reaction is triggered only by those catalysts for which the thiol groups are spontaneously oxidized to sulfonic groups during the gold immobilization process, i.e., upon contacting the gold-containing essential oil phase with the SH-SBA-15 material. Moreover, it has been observed in these cases that the increase in catalytic activity runs parallel with the agglomeration of gold clusters to render nanoparticles [8].

These studies evidence the complexity of the overall catalytic reaction, and brought us to investigate further the influence of some properties of the catalyst that might be determinant for the reaction output. First, we wondered whether an SBA-15 morphology other than the conventional rod-like particles we have reported previously [8] might have an influence on the overall catalyst performance. In these particles, the channels extend along their main axis. In this way, and in order to facilitate the diffusion in the interior of the mesopores, we have prepared functionalized SBA-15 materials possessing short channels by using the non-ionic block copolymer surfactant Pluronic P104 ((EO)₂₇(PO)₆(EO)₂₇, where EO and PO stands for ethylene and propylene oxide, respectively), instead of the higher molecular weight Pluronic P123 used previously, in conditions similar to those previously reported for all-silica materials [12,13]. In this case, as it will be shown below, SBA-15 particles with plate-like morphology have been achieved, where the channels run perpendicular to the basal plane of the platelets. Second, as far as oxidized sulphur species seem to be required for Au activity [8], we have intentionally pre-oxidized the SBA-15 materials bearing -SH groups before contacting them with the gold solution by using two different oxidation reagents and procedures, namely hydrogen peroxide, which has been used previously to oxidize thiol to sulfonic acid in MCM-41 [14,15] and SBA-15 [16], and dimethyldioxirane, which is able to oxidize thiol groups to sulfones and -SO₃⁻ groups [17,18]. Finally, it has to be considered that the catalytic cyclohexene oxidation reaction involves molecules with very different polarity, i.e. cyclohexene and its two main and more polar oxidation products, cyclohexenol and cyclohexenone [8]. Therefore, it could be hypothesized that the modification of the hydrophobicity of the catalysts would have an impact on their performance. In order to explore this hypothesis, SBA-15 precursor materials of desired morphology were synthesized by a co-condensation method by using mercaptopropyl and alkyl (propyl and octyl) hydrophobic groups. The Au-containing materials derived from these precursors have been tested as catalysts for the oxidation of cyclohexene with oxygen in liquid phase at atmospheric pressure.

2. Experimental

2.1. Synthesis of thiol-functionalized short-channel SBA-15 silica

Synthesis of short-channel SBA-15 silica functionalized solely with thiol and with both thiol and alkyl groups was carried out by a method adapted from that reported for pure silica materials [12,13]. These hybrid SBA-15 materials were prepared from gels with molar composition: 1.0 TMOS: 0.05 MPTMS: x R: 0.077 P104: 6.27 HCl: 303 H₂O,

where TMOS stands for tetramethyl orthosilicate (Sigma-Aldrich, > 99%); MPTMS for 3-mercaptopropyltrimethoxysilane (Sigma-Aldrich, 95%); R for either propyltrimethoxysilane (TMPS, Sigma-Aldrich, > 99%), or octyltriethoxysilane (OTES, Alfa Aesar, 95%), and x = 0 or 0.05; P104 for Pluronic P104, the triblock co-polymer (EO)₂₇(PO)₆(EO)₂₇, (Sigma-Aldrich); and HCl for hydrochloric acid (Panreac, 37 wt.%). The HCl and H₂O content of the gel containing TMPS were optimized to 5.41 and 178 mol per mole of TMOS, respectively, in order to improve the ordering of the recovered SBA-15 material. The procedure to prepare the material functionalized with MPTMS was as follows. 170 mL of 1.1 M HCl were placed in a pyrex bottle provided with a stirring bar, and 3 g of P104 were added. Once the surfactant was dissolved, 4.4 mL of TMOS and 0.260 mL of MPTMS were added. For the preparation of propyl- and octyl-functionalized materials, the corresponding amount of TMPS and OTES were added in this step. Then, the mixture was stirred for 24 h at room temperature. After this, the closed bottle was heated at 80 °C (or 60 °C for the TMPS gel) for 5 days. After that, the bottle was cooled down to room temperature and its content filtered, washed with water and ethanol and dried at room temperature overnight. The dried sample was treated with ethanol (100 mL of ethanol per g of sample) under stirring in a 1 L round-bottom flask at 90 °C for 4 h, in order to remove the surfactant. The resulting samples were denoted as SH for the as-made material functionalized with SH groups only; SPr for that functionalized with both SH and propyl groups, and SOc for the material resulting from gels containing both SH and octyl groups. In all cases, the suffix “ext” is added after the name for the samples treated with ethanol to remove the surfactant, i.e. SH-ext and so on.

2.2. Oxidation of thiol-SBA-15 supports with hydrogen peroxide

0.5 g of the extracted SBA-15 materials were oxidized with 15 mL of a 15 wt.% H₂O₂ solution in water under stirring for 24 h, and the resulting solid was filtered and washed with water, treated with diluted sulfuric acid, washed again with water and dried at room temperature. The resulting samples were denoted as SH-hp, SPr-hp and SOc-hp, where “hp” stands for hydrogen peroxide.

2.3. Oxidation of thiol-SBA-15 supports with dimethyldioxirane

A solution of dimethyldioxirane (DMD) in acetone was first prepared according to the following procedure [18]: a 2 L three-necked round bottom flask was provided with a magnetic bar for magnetic stirring, introduced in an ice bath and connected to a two-necked receiving flask. Then, 254 g of water, 192 mL of acetone and 58 g of NaHCO₃ were added. Under vigorous stirring, 120 g of oxone (2KHSO₅·KHSO₄·K₂SO₄, Alfa Aesar, 99.9%) were added slowly in portions at 3 min intervals. After this, a moderate vacuum was applied, the ice bath removed and the collecting two-necked flask introduced in a dry ice/ethanol bath, and the dimethyldioxirane/acetone solution gently distilled and collected in the cooled flask (-78 °C). The product is stored at 23 °C. Then, 0.7 g of the extracted SBA-15 supports were treated with 15 mL of the DMD acetone solution under stirring at room temperature for 24 h, in a 25 mL Erlenmeyer flask covered with Parafilm. The reaction mixture was then filtered, washed with acetone and dried at room temperature. The samples were denoted SH-DMD, SPr-DMD and SOc-DMD.

2.4. Synthesis of the gold entities

The gold nanosized entities were prepared from a two-liquid phases system according to a method previously described [4,8]. In a typical procedure, a gold lump (0.094 g, Johnson-Matthey, 99.99%) was dissolved under gentle stirring in 34 g of *aqua regia*, prepared by mixing (4:1, w/w) nitric acid (Panreac, 65 wt.%) and ammonium chloride (Sigma-Aldrich, > 98 wt.%), while heating at 40 °C in a sand bath. After

cooling, the resulting golden yellow solution was placed in a 100 mL decanting funnel, and then 17 g of rosemary essential oil were gently added, which remained as a top layer over the gold solution. The system was then left at room temperature undisturbed, i.e., the two liquid phases were not mixed, and aliquots of the organic layer were taken at the desired time to prepare the Au-SBA-15 materials, as it is described below. The rosemary essential oil was supplied by the Spanish company El Granero Integral (The Integral Barn) and its chemical composition [4,8] was determined by GC-MS employing a gas chromatograph (Agilent 6890) coupled with a mass spectrometer (Agilent 5973N) using a capillary column made of methylpolysiloxane (30 m \times 0.25 mm \times 0.25 μ m), heating from 70 to 290 °C at 6 °C/min. The oil composition (in wt%) was: 24.9% 1,8-cineole, 21.9% *alpha*-pinene, 20.91% camphor, 9.06% camphene, 3.81% borneol, 3.34% verbenone, 2.59% myrcene, 2.41% *beta*-pinene, 2.01% caryophyllene, 2.00% *p*-cymene, 1.16% *alpha*-humulene, 0.98% bornyl acetate, 0.94% *gamma*-terpinene, 0.63% 4-terpineol, 0.63% *alpha*-terpineol, 0.29% *alpha*-terpinolene, 0.28% fenchone.

2.5. Immobilization of the gold entities on SBA-15

Aliquots of 3.75 mL of the organic layer were taken after 24 h of addition of the rosemary oil to the gold solution and each of them was mixed with 18.75 mL of ethanol. To this solution, 0.5 g of the SBA-15 materials were added and the mixture was stirred at room temperature for 4 h. After that, the solid was separated by centrifugation and washed with four portions of 40 mL of ethanol each. The corresponding Au-containing samples were denoted as SH-Au, SH-hp-Au, SPr-Au, and the like. The routes followed to prepare the catalysts are displayed in Scheme 1.

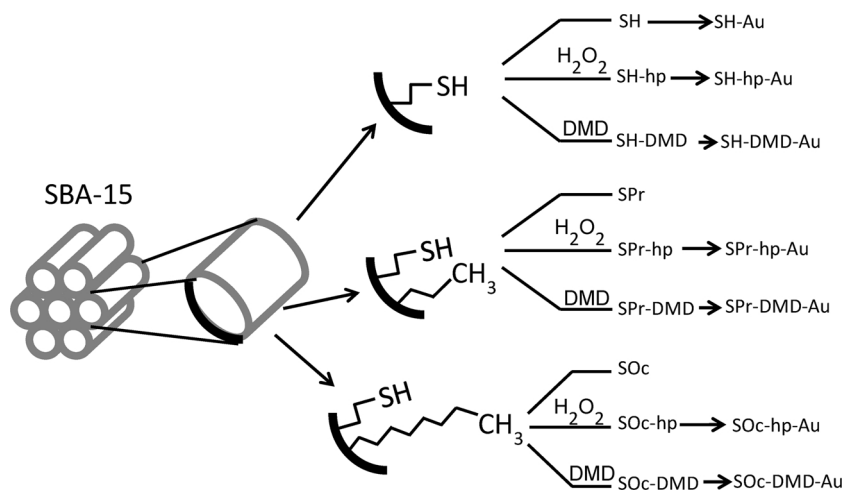
2.6. Catalytic tests

The oxidation of cyclohexene with molecular oxygen was carried out by the procedure described in [8], which was developed from that reported in [19]. The catalytic reaction was carried out in a 50 mL glass four-neck round-bottom flask, provided with a condenser through which water at 5 °C was circulated to minimize the evaporation of reagents and products. The flask was immersed in a silicone oil bath to keep the reaction temperature at 65 °C, measured inside the reaction mixture by a thermometer inserted in one of the necks. The experimental set-up was not protected against environmental light. The reaction mixture was made of 5.6770 g of cyclohexene (0.0676 mol, Sigma-Aldrich, 99%), 0.5677 g of octane (10 wt.% referred to cyclohexene; Sigma-Aldrich, > 99%), 0.2839 g of a *tert*-butyl hydroperoxide

solution (TBHP, 5 wt.% referred to cyclohexene; ~5.5 M in decane, Sigma-Aldrich), 4.2578 g of toluene (75 wt.% of the cyclohexene; Panreac, > 99.5%), and 0.070 g of catalyst. O₂ (1.8 mL/min) was bubbled through the stirred reaction mixture. The catalysts were previously heated at 100 °C for 1 h in the reaction flask equipped with a tube containing molecular sieve 5A in order to remove the traces of water coming from the catalysts, subsequently cooled down to the reaction temperature of 65 °C, and then the reagents were added. The trap was removed and replaced by the condenser before the reaction started. We have decided to follow ref. [19] on the use of TBHP as initiator, although the same group reported later that oxidation reactions can be carried out free of initiator [20] provided the cyclohexene does not contain a chemical stabilizer. However, the subject is still controversial (see [21] and references therein). As we cannot guarantee our cyclohexene source is stabilizer-free, we have preferred to keep using TBHP as in our previous investigation [8]. Aliquots of 0.20 mL of the reaction mixture were taken at given time intervals, filtered through a 4 mm PTFE filter of 0.45 μ m and analysed by GC in a Varian CP-300 instrument, by using a FactorFour™ (Varian VF-1 ms) dimethylpolysiloxane capillary column of 15 m of length and 0.25 mm of i. d. Octane was used as internal standard. Five reaction products were identified, two of them resulting from the addition of oxygen to the cyclohexene double bond, namely cyclohexene epoxide and cyclohexanediol, and three coming from the allylic oxidation of the cyclohexene ring: 2-cyclohexen-1-ol, 2-cyclohexen-1-one and 2-cyclohexenyl hydroperoxide. Cyclohexene conversion was calculated from the yields of these five products.

2.7. Characterization techniques

Powder X-ray diffraction was carried out using a PANalytical X'pert Pro instrument (Cu K α radiation). Gold content of the solid was determined by inductively coupled plasma (ICP-OES) spectrometry with an ICP PlasmaQuant PQ 9000 Analytik Jena spectrometer. Thermogravimetric analyses were performed in a Perkin-Elmer TGA7 instrument, in air (40 mL/min) with a 20 °C/min heating ramp from 25 to 900 °C. CHNS elemental analyses were done in a LECO CHNS-932 analyser provided with an AD-4 Perkin-Elmer scale. Nitrogen adsorption-desorption isotherms were measured in a Micromeritics ASAP 2420 apparatus at the temperature of liquid nitrogen (-196 °C). The samples were degassed in situ at 70 °C in vacuum for 16 h prior analysis. Surface area was determined using the BET method. The pore volume and the average pore diameter were calculated by applying the BJH protocol to the adsorption branch of the isotherm. Diffuse reflectance UV-vis (UV-vis) spectra were recorded on a Cary 5000 Varian



Scheme 1. Routes followed to prepare SBA-15 samples functionalized with mercaptopropyl (and alkyl) groups, their oxidized counterparts and corresponding gold-containing catalysts.

spectrophotometer equipped with an integrating sphere with the synthetic polymer Spectralon as reference. The data were expressed in absorbance units. MAS NMR spectra were recorded with a Bruker AV 400 WB spectrometer. ^1H to ^{13}C cross-polarization (CP) spectra were recorded using a $\pi/2$ rad pulses of 4.5 μs for ^1H , a contact time of 5 ms and a recycle delay of 3 s. For the acquisition of the ^{13}C spectra, the samples were span at a rate of 5–5.5 kHz. ^{29}Si MAS NMR spectra were recorded at 79.5 MHz using a 4 mm probe. Transmission electron microscopy studies were carried out using a JEOL 2100F electron microscope operating at 200 kV. The catalysts were dispersed in ethanol and dropped onto a holey carbon copper grid for the observations. Scanning electron microscopy was carried out using a Field Emission Phillips XL30 S-FEG instrument. The samples were coated with Cr before observation.

X-ray photoelectron spectra (XPS) have been collected using a SPECS instrument with UHV system (pressure in the range of 10^{-10} mbar), equipped with a PHOIBOS 150 9MCD energy analyzer. A non-monochromatic Mg K_{α} (1253.6 eV) X-ray source was used, working at a power of 200 W, with an acceleration voltage of 12 kV. High-resolution regions were recorded with a pass energy of 20 eV. For analysis, the powder samples were pressed into self-supporting wafers and stuck on the sample holder with double-sided adhesive conductive carbon tape. Spectra were referenced against the O 1s emission line (binding energy set to 532.9 eV) to correct for charging effect. Decomposition of experimental peaks into components (70% Gaussian, 30% Lorentzian) was done using a non-linear, least squares fitting algorithm and a Shirley baseline. Relative atom ratios were calculated from the sum area of the core-level components of Si, S and Au, using the relative sensitivity factors provided by Casa XPS software.

3. Results and discussion

3.1. Extracted samples

The XRD pattern of the extracted thiol-containing SH material (Fig. 1) shows the profile characteristic of SBA-15 mesostructure, with an intense d_{100} reflection and unit cell parameter (a_0) of 10.1 nm (Table 1). The introduction of propyl and octyl groups together with mercaptopropyl produces a visible broadening of the d_{100} reflection, which suggests that the alkyl groups have been effectively incorporated in the co-condensation process of the corresponding alkoxy silanes and are present in the pore surface in addition to mercaptopropyl moieties, perturbing somehow the micellar arrangement of the P104 molecules that built up the structure. The surface area decreases with the incorporation of alkyl groups and the effect is more pronounced as the

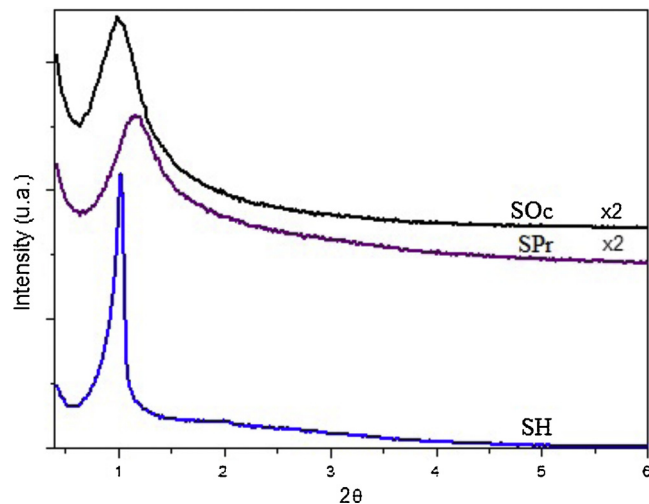


Fig. 1. XRD patterns of samples SH-ext, SPr-ext and SOc-ext.

Table 1

Structural properties of the as-made materials and structural and textural characteristic of the extracted samples.

Sample	d -Spacing $d_{100}(\text{nm})$	Unit cell parameter $a_0(\text{nm})$	S_{BET} (m^2/g)	V_p (cm^3/g)	D_p (nm)
SH	8.72	10.1			
SH-ext	8.69	10.0	661	0.55	4.5
SPr	7.79	9.0			
SPr-ext	7.60	8.8	497	0.34	2.6
SOC	10.2	8.9			
SOC-ext	9.6	8.3	426	0.40	3.2

hydrocarbon chain length increases. The pore size of SH is 4.6 nm, and it is reduced to ~ 3 nm for the samples prepared from propyl (SPr) and octyl (SOC) containing gels, which again suggests their effective incorporation into the pores, decreasing in this way their average free diameter.

The inspection of the SH-ext sample by TEM reveals the presence of some particles with thin plate shape and developed (001) faces (Fig. 2a). Moreover, it shows a very well ordered hexagonal arrangement of pores, as evidenced also by the electron diffraction pattern obtained along the channel direction (inset in Fig. 2a). Long rod-like particles have never been observed. The platelets exhibit a small thickness, with a maximum of 300–400 nm, consistent with the thickness of the all-silica SBA-15 platelet particles and the nanorods forming those particles described previously [12,13]. The images taken perpendicular to the channel direction (Fig. 2b) show that the channels run along the short dimension of the platelets. TEM images of the two alkyl-containing samples, SPr-ext and SOC-ext, show the presence of very tiny particles of irregular morphology whose size is < 200 nm, with a relatively disordered arrangement of pores, in agreement with their XRD pattern discussed above. SEM images (Fig. 3) confirm the presence of particles of irregular shape in the SPr and SOC samples, with sizes in general below 200 nm, being somewhat larger in the former. Moreover, no rod-like particles have been found. Therefore, regardless the perfection of the hexagonal pore arrangement and the fact that for the two samples functionalized with propyl and octyl groups no plate-like particles have been formed, in all these cases SBA-15 particles having short channels have been achieved, which was one of the main goals of the research. However, further investigation would be needed in order to improve the pore arrangement and particle morphology for these functionalized materials.

The presence of sulphur in the three samples suggests the effective incorporation into the solid of the mercaptopropyl groups present in the synthesis gel, but it can be observed that the amount of this element slightly decreases from 1.78 wt.% for SH, to 1.51 wt.% and 1.39 wt.% for the samples prepared from gels containing octyl (SOC) and propyl (SPr) groups, respectively (Table 2). This evidences a competition between the two functional groups for their incorporation into the SBA-15 structure. It can be seen also in Table 2 that the C/S ratio is higher than that of the propylthiol moiety, which suggests that other carbon compounds are present in the materials. Indeed, the ^{13}C CP MAS NMR spectra that will be discussed below show the presence of ethoxy groups, as well as some minor amount of residual surfactant. TG analysis of sample SH (Fig. 4) shows a weight loss at $T < 100$ °C attributed to water desorption, and a sharp one at higher temperature, centered at 320 °C, which can be assigned to the desorption/combustion of propylthiol groups in SBA-15 materials [8,16]. The samples functionalized with alkyl groups in addition to mercaptopropyl present TG patterns qualitatively similar to that of SH (Fig. S1 of Supplementary information for sample SPr and Fig. S2 for sample SOC), but the weight loss centered at ~ 300 °C increases with the chain length of the hydrocarbon moiety (Table 2). This increase of weight loss is more relevant if it is taken into account that the amount of sulphur decreases in the same way. This behavior suggests that the mercaptopropyl and alkyl moieties

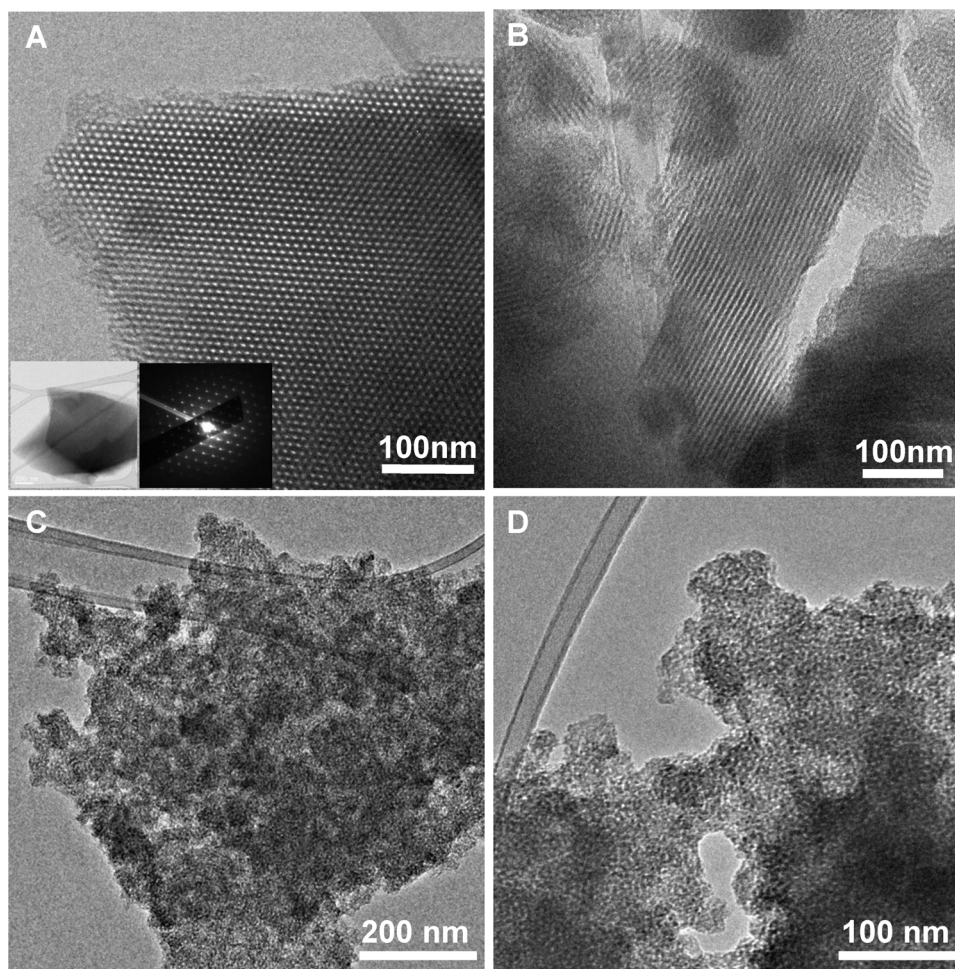


Fig. 2. (A) TEM Images of sample SH-ext along the channel direction showing the hexagonal packing of the pores. Low magnification particle morphology and electron diffraction pattern are included in the insets corroborating that the channels are running along the short dimension of the crystals, which are close to hexagonal plates. (B) TEM image of sample SH-ext perpendicular to the channels, (C) sample SOc-ext and (D) sample SPR-ext.

are desorbed/decomposed at roughly the same temperature, and that at least part of the extra-weight loss of these two samples as compared to SH could be attributed to alkyl chains present in the structure, although the co-existence of several organic species in the material preclude a quantitative determination of their content. ^{13}C CP MAS NMR will show the effective incorporation of hydrocarbon moieties in the samples.

3.2. Oxidized samples

Oxidation of the extracted samples with either hydrogen peroxide or dimethyldioxirane (DMD) produced significant changes in the nature of the samples that can be monitored by a combination of chemical and thermal analysis, XPS and NMR spectroscopy. Significant differences have been found in the way the two oxidation procedures affect the starting materials. The first observation common to all oxidized samples is that none of the oxidation procedures removed sulphur in a significant manner, as the content of this element is quite similar to that of the extracted samples (Table 2). The consequence of the oxidation process on the nature of the functional groups present in the solid can be conveniently monitored by ^{13}C CP MAS NMR spectroscopy (Fig. 5). In the spectrum of sample SH, resonance signals at 11 ppm and ~ 26 ppm correspond, respectively, to the carbon atom attached to Si in the mercaptopropyl moiety and the two remaining carbon atoms of the propyl chain [22,23]. The signals at 59 ppm and 16 ppm correspond, respectively, to the C atom attached to oxygen and the terminal methyl groups in the $-\text{O}-\text{CH}_2-\text{CH}_3$ ethoxy group [23]. These groups are

formed by reaction of the hot ethanol used to remove the surfactant with the silanol groups present in the as-made material. Finally, the band at 70 ppm corresponds to residual surfactant [23]. Oxidation of this sample with hydrogen peroxide largely removed the 26 ppm band, while new ones appeared at 54 ppm and 18 ppm. The former has been assigned to the α carbon atom attached to the sulfur atom in the sulfonic acid group, and the latter to the β carbon atom of the propyl sulfonic group [23], while the C atom bonded to Si is responsible for the 11 ppm resonance. The bands at 16 ppm and 70 ppm are associated to residual surfactant. It is interesting to notice that the oxidation treatment largely decreases the intensity of the bands associated to ethoxy groups, in agreement with the chemical analysis. If the sample is oxidized with DMD, the band at 26 ppm corresponding to the mercaptopropyl group is completely removed, while a new and intense one appears at 54 ppm, as well as another one at 18 ppm, while that at 11 ppm remains unchanged. It has been reported that dimethyldioxirane is a very efficient agent for the oxidation of organic sulfides and thiol groups to sulfone and sulfonic groups [18], and hence these three bands at 54, 18 and 11 ppm should correspond, respectively, to the C atoms in α and β positions of the propylsulfonic moiety and to the C atom linked to the Si atom. Moreover, the DMD treatment removes all the ethoxy groups, as the resonances of the corresponding C atoms have vanished.

The oxidation of the thiol groups has also been monitored by XPS. Fig. 6 shows the S 2p core level spectra of sample SH-ext before and after DMD oxidation. The broad peak of the SH-ext sample is asymmetric in the low binding energy (BE) side, which evidences that it

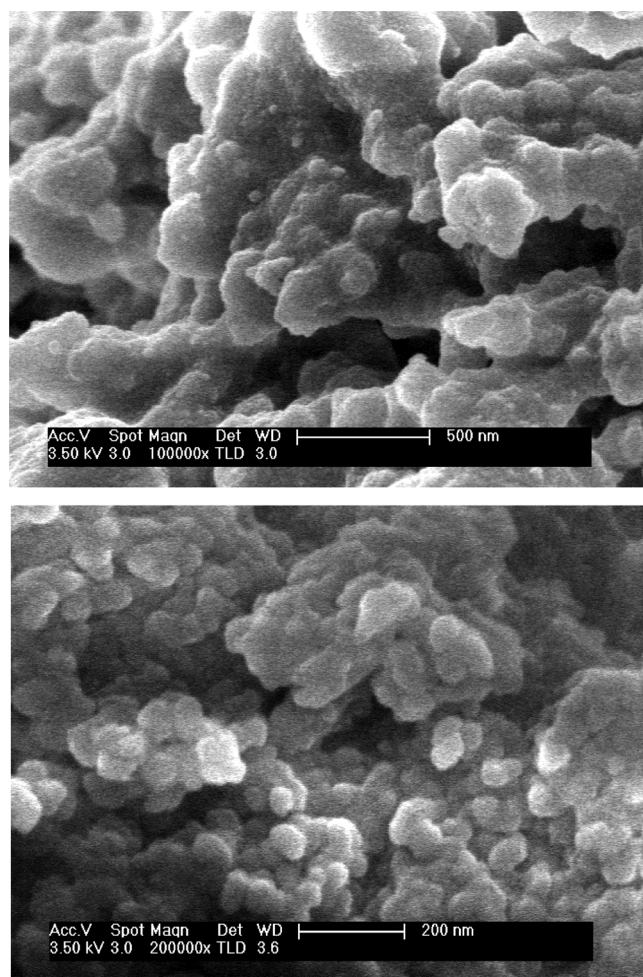


Fig. 3. SEM images of samples SPR-ext (top) and SOc-ext (bottom).

Table 2
Chemical composition (wt.%) and TG analysis results (wt.%) of supports.

Sample	C	H	S	C/S ^a	Weight loss T < 140 °C	Weight loss T > 140 °C
SH-ext	6.38	2.48	1.78	9.56	5.75	17.07
SH-hp	8.18	2.7	1.67	13.05	8.47	15.89
SH-DMD	7.95	3.47	1.47	14.43	14.72	20.90
SPr-ext	10.57	3.20	1.39	20.30	6.59	21.30
SPr-hp	5.99	2.35	1.25	12.77	7.15	14.31
SPr-DMD	7.67	2.97	1.40	14.59	9.37	18.68
SOc-ext	14.98	3.54	1.51	26.44	4.32	28.05
SOc-hp	13.30	3.28	1.51	23.48	5.06	24.47
SOc-DMD	14.37	3.50	1.43	26.79	3.57	27.65

^a Mol ratio.

envelopes the S 2p_{3/2} and S 2p_{1/2} components with 2:1 intensity ratio due to the characteristic spin-orbit splitting [24]. The BE at the maximum intensity of the peak, which is mostly contributed by the S 2p_{3/2} component, is 163.5 eV, which corresponds to SH groups [25]. After oxidation of this sample with DMD, this peak disappears completely and it is replaced by a new one at higher BE, also asymmetric and tailed at the low BE side, centered at 168.8 eV. Unresolved S 2p peaks at 168.0 eV have been assigned to sulfone -S(O)₂- group in poly(ether sulfone) [26]. S 2p_{3/2} peaks at BE in the range 168.1–168.5 have been assigned to sulfonic [25] or sulfonate group -SO₃⁻ [27], and it has been also reported that the BE of the sulfonate group is sensitive to the counteraction [28]. Therefore, the BE of 168.8 eV can be assigned to S (VI) chemical species and evidences that DMD oxidizes quantitatively

thiol to sulphur species in high oxidation state. Moreover, the BE value is closer to that of -SO₃⁻ than to sulfone. In order to distinguish between both groups, the acidity of the solid has been determined by base titration, and it has been found to be quite similar to that of the sample treated with hydrogen peroxide, which contains sulfonic groups. Therefore, -SO₃⁻ species would be present in the sample treated with DMD. It can be seen in Table 3 that the S/Si atom ratio at the surface is nearly half that of the bulk, which indicates a concentration gradient of sulphur across the SBA-15 particles that would have a S-rich inner core.

The occurrence of silane units in the extracted and oxidized samples can also be monitored by ²⁹Si MAS NMR (Fig. 7). The signals appearing in the spectra at -92, -101 and -110 ppm correspond to Q², Q³ and Q⁴ species, respectively, where Qⁿ refers to [Si(OSi)_n(OH)_{4-n}] environments, with n = 0, 1, 2, 3 and 4. It can be noticed the high concentration of silanol Si-OH groups, as evidenced by the intensity of the corresponding -101 ppm signal. The resonance at -66 ppm is attributed to T³ sites, silane species (those having C-Si bonds) in environments described as RSi(OSi)₃ [29,30].

The oxidation of the samples also leaves its footprint in the TGA profile (Fig. 4), which contributes to clarify further the outcome of the oxidation process. For SH sample, oxidation with hydrogen peroxide gives rise to a new weight loss centered at ~250 °C, while that corresponding to thiol groups decreases in intensity but it is still clearly visible as a sharp thermal event centered at 330 °C. Thermal events at 230 °C–260 °C are associated to the presence of sulfonic moieties in mesoporous materials and sulfonic resin Amberlyst-15 [8,16]. The total weight loss at T > 140 °C is smaller than that of the extracted material, owing to the removal of the ethoxy groups, in agreement with the NMR results. It can be also noticed that the amount of adsorbed water (weight loss at T < 140 °C) increases with the treatment. From these results, it could be concluded that the treatment of this sample with hydrogen peroxide only oxidized partially the thiol to sulfonic acid. However, oxidation with DMD produces deeper changes in the TGA pattern (Fig. 4, SH-DMD sample). In this case, two high-temperature thermal events are identified, centered at ~270 °C and 500 °C, being the former more intense than the latter, while no event associated to the presence of thiol groups is observed. Moreover, the most intense weight loss in mesoporous SBA-15 materials containing sulfonic groups occurs at T ~ 350 °C [8,13]. Then, this result confirms the effective oxidation of thiol to sulfonic groups, in agreement with the XPS results discussed above.

As we have seen that the chemical changes produced in the thiol groups by the oxidation treatments can be conveniently monitored by TG, we have used this methodology to check their effect on the two samples functionalized with propyl (SPr) and octyl (SOc) groups in addition to mercaptopropyl. The TGA pattern of the SPr sample oxidized with hydrogen peroxide (SPr-hp in Fig. S1) strongly resembles that of sulfonic acid-containing materials, with thermal events associated to the decomposition/oxidation of organic material detected at 250 °C, 370 °C (being this one the most intense) and 510 °C. This evidences an efficient oxidation of thiol to sulfonic acid groups. The TG profile of the sample treated with DMD is quite similar to that of sample SH-DMD, suggesting again the presence of sulfonic groups, although the main weight loss shifts to slightly higher temperature and is centered at 320 °C. Finally, the treatment of sample SOc with H₂O₂ does not reveal significant changes in the TGA pattern (Fig. S2), other than reducing the weight loss at T > 140 °C. This evidences that the treatment is not suitable for oxidizing the thiol groups in this case. The presence of long C8 hydrophobic alkyl chains in the material might reduce the ability of hydrophilic hydrogen peroxide to reach the thiol groups located at the surface, under the conditions described in this work. The higher hydrophobicity of this sample as compared with that of SH and SPr materials is evidenced by its much lower amount of adsorbed water, as revealed by the weight loss at T < 140 °C, (Table 2). However, DMD is as efficient as it was for the two other samples to oxidize thiol to sulfonic groups, being the TGA pattern quite similar to that of sample SH-

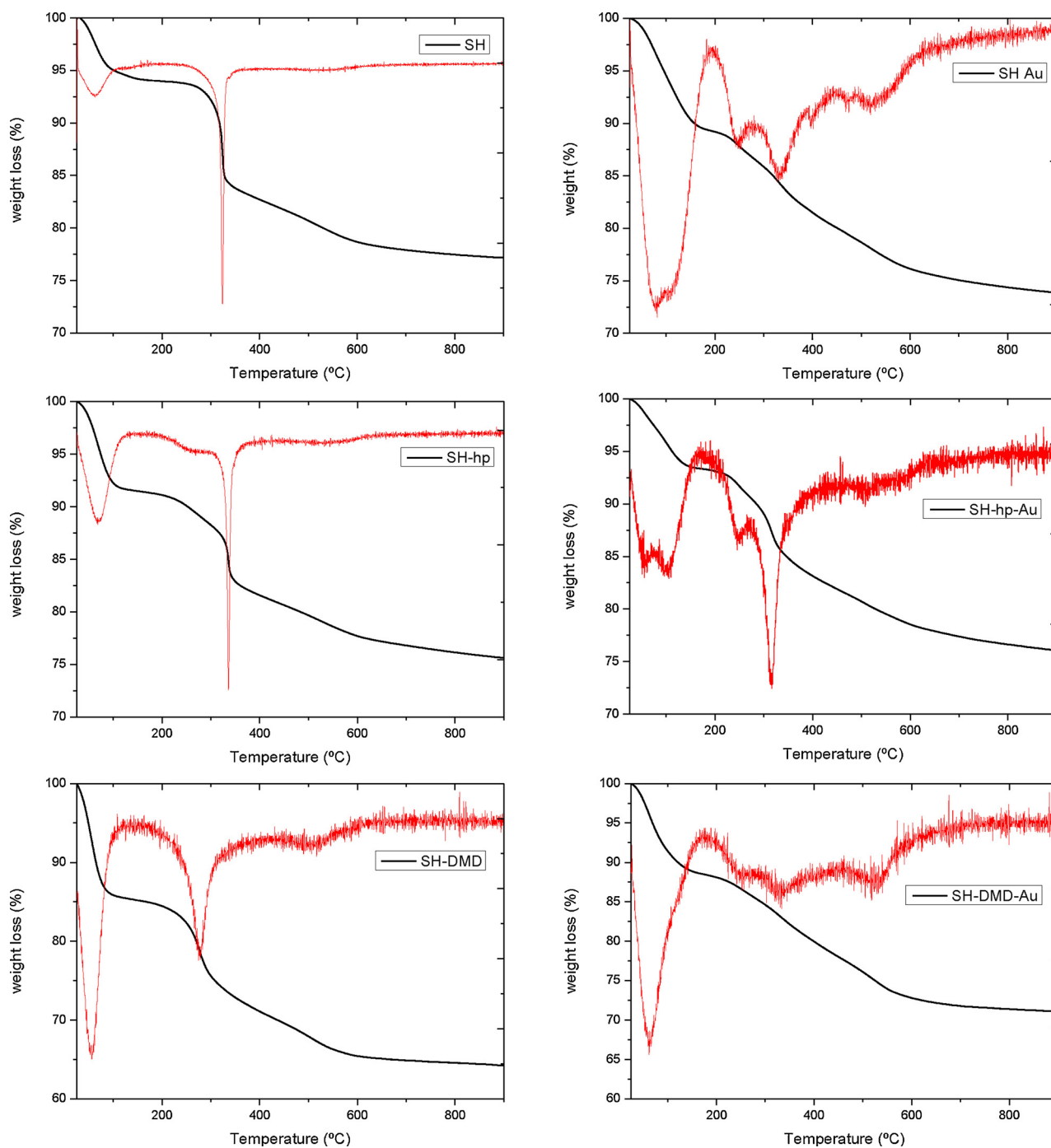


Fig. 4. TGA/DTG curves for SH samples (left) and the corresponding Au-containing materials (right).

DMD.

3.3. Gold-containing materials

SH-ext and all the oxidized samples put in contact with aliquots of the rosemary oil solution as described in the experimental section are able to immobilize gold, whose amount varies for different materials (Table 4). It is nearly 1.1 wt.% for sample SH, and it slightly decreases for its corresponding oxidized materials, but it is similar for both of them. Pre-oxidation of sample SP_r with H₂O₂ does not change its ability to capture gold from the rosemary solution, as the metal content is quite similar to that of sample SH. However, pre-oxidation with DMD clearly reduces the gold content (0.46 wt.%). A similar though more marked

trend is found for oxidized SOc material containing octyl groups, as in this case the amount of gold in SOc-DMD sample is further reduced to only 0.23 wt.%, and pre-oxidation with H₂O₂ already decreases it to 0.7 wt.%. The sulphur content remains nearly unchanged after Au immobilization, and the S/Au ratio of the samples is in the range 8–40. For some of them, a small increase in the total carbon content is found (Table 4).

The XPS spectrum of sample SH-Au (Fig. 6) shows the presence of two S 2p peaks at BE energies 163.6 eV and 168.1 eV, being the intensity of the last one 57% of the total S intensity. The low BE peak corresponds to thiol groups still present in the sample, while the high BE peak is assigned to S in $-\text{SO}_3^-$, as it was discussed above. This evidences that a major fraction of the thiol groups present on the

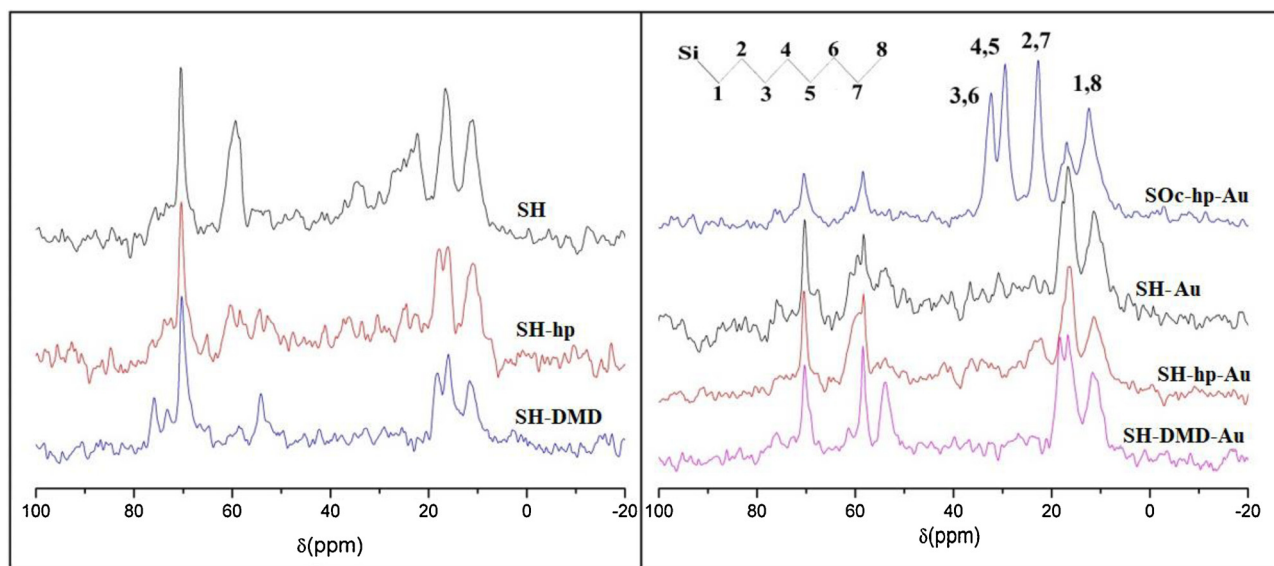


Fig. 5. ^{13}C MAS NMR spectra of selected samples before (left) and after (right) gold immobilization.

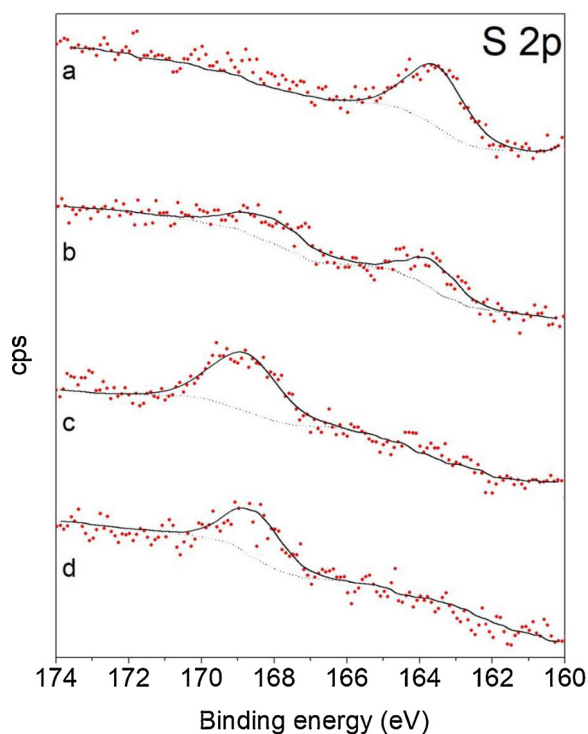


Fig. 6. S 2p core-level spectra of samples (a) SH-ext, (b) SH-Au, (c) SH-DMD and (d) SH-DMD-Au. Scatter points correspond to raw data and lines to curve-fitting results.

sample surface has been oxidized upon contacting the material with the Au-containing essential oil layer. The oxidant activity of the essential oil that has been in contact with the solution of gold in *aqua regia* should be linked to the changes that we have observed in its colour as a function of time. The oil starts to acquire a deep reddish coloration after one hour, becoming brown-red after one day (Fig. S3). These changes strongly suggest that the terpenic compounds initially present in the oil would react with the strongly acidic and oxidant solution of gold in *aqua regia*, and the compounds resulting from this reaction (which have not been identified yet) should be able to oxidize thiol to sulfonic groups. The S 2p spectrum of the SH-DMD-Au (Fig. 6) is quite similar to the corresponding sample before Au immobilization, evidencing the presence of $-\text{SO}_3^-$. We do not observe in the spectrum any S 2p signal at BE < 163.0 eV that would eventually be associated to S-linked to Au [24], within the resolution power and sensitivity of our XPS instrument. It will be shown below that the S/Au surface ratio is $\gg 1$, and then most of the S atoms would not be involved in Au binding, and therefore the overwhelming majority of S-free groups would overshadow S atoms eventually involved in Au binding.

The gold immobilization process produced in general noticeable changes in the TGA patterns of the samples, which can be interpreted on the basis of the changes in the chemical nature of the S-bearing groups revealed by the XPS spectra. The TG profiles of the SH samples, whether pre-oxidized or not, are quite similar (Fig. 4). The weight loss at $T < 160^\circ\text{C}$ is composed of two thermal events, one at lower T due to water desorption, and the other centered at $T \sim 100^\circ\text{C}$, probably arising from the desorption of more strongly held water or eventually from volatile organic products deposited in the materials during the immobilization of gold. Several thermal events can be distinguished at higher temperature, centered at $\sim 240^\circ\text{C}$, $\sim 330^\circ\text{C}$ and $\sim 520^\circ\text{C}$, being

Table 3
XPS results.

Sample	BE (eV)			Surface atomic ratio			Bulk atomic ratio	
	S 2p	Au 4f _{7/2}	Au 4f _{5/2}	S/Si	Au/Si	S _{ox} /S ^a	S/Si	Au/Si
SH-ext	163.5	–	–	0.020	–	0	0.043	–
SH-Au	163.6	84.5	88.1	0.018	0.0012	0.57	0.043	0.0046
SH-DMD	168.1	–	–	0.024	–	1	0.043	–
SH-DMD-Au	168.5	84.6	88.2	0.015	0.0028	1	0.041	0.0038

^a Fraction of oxidized sulphur species.

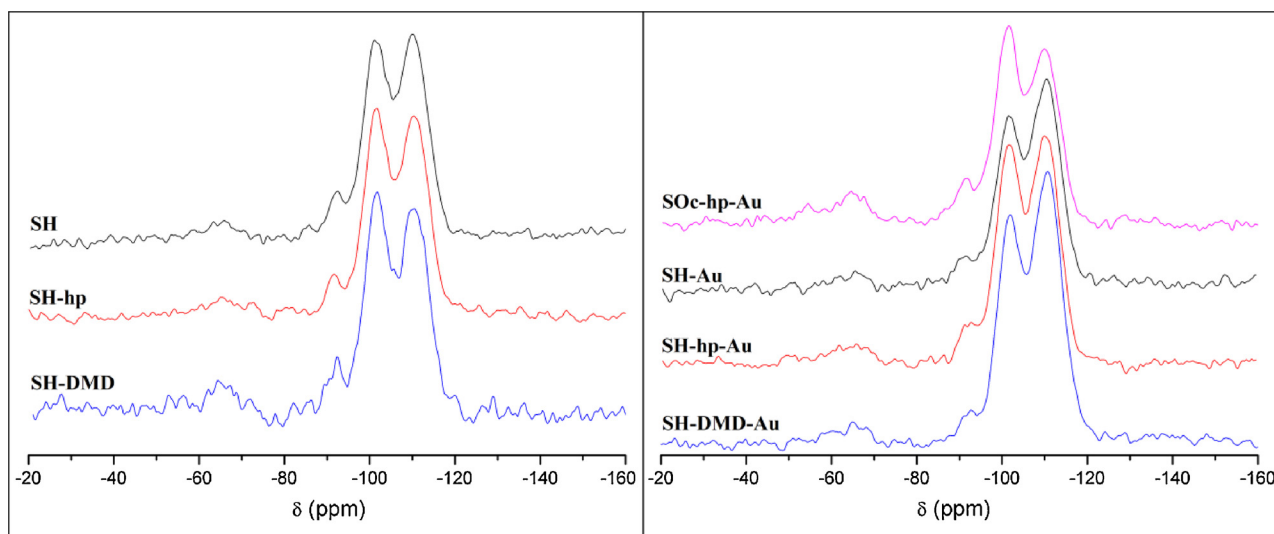


Fig. 7. ^{29}Si MAS NMR spectra of selected samples before (left) and after (right) gold immobilization.

Table 4

Chemical composition (wt.%) and TG analysis results (wt.%) of Au-containing materials.

Sample ^a	C	H	S	Au	C/S ^b	Weight loss T < 140 °C	Weight loss T > 140 °C
SH-Au	10.13	2.91	1.67	1.09	16.17	10.65	15.46
SH-hp-Au	10.27	2.73	1.66	0.82	16.49	6.64	17.28
SH-DMD-Au	8.35	2.98	1.55	0.87	14.37	11.42	17.46
SPr-hp-Au	8.25	2.74	1.32	1.17	16.64	10.93	15.22
SPr-DMD-Au	8.94	3.02	1.41	0.46	16.89	10.61	18.80
SOc-hp-Au	13.40	3.26	1.51	0.70	23.66	7.41	22.05
SOc-DMD-Au	12.67	3.36	1.48	0.23	22.80	7.16	19.95

^a Traces of N ranging from 0.1 wt.% to 0.5 wt.% are found in the samples.

^b Mol ratio.

most pronounced the second one. These events are characteristic of sulfonic groups, as it has been discussed above. However, only in sample SH-DMD-Au all S-bearing groups have been shown by XPS to belong to $-\text{SO}_3^-$ species, and therefore it should be associated to the smooth weight loss observed at $\sim 330^\circ\text{C}$. In contrast to this, a more intense 330°C step is observed in sample SH-Au, which still contains thiol groups as evidenced by XPS, whereas for sample SH-hp-Au the second weight loss is even steeper and closer to 300°C . These TGA features suggest that part of the thiol groups might still be present in the two last samples. We have reported previously [8] that the rosemary oil phase put in contact with the gold *aqua regia* solution for one day is not able to oxidize the mercaptopropyl groups present in conventional SBA-15 materials having rod-shape morphology, containing therefore very long channels. Then, it can be concluded that the oxidation of thiol groups is facilitated by the much shorter channels existing in the SH sample, although the oxidation is not complete, as thiol groups remain in the Au-materials. TGA profiles of the propyl-(SPr) and octyl-(SOc) samples are qualitatively similar to those of SH materials (Figs. S1 and S2), although sample SOc-hp-Au still shows a narrower weight loss centered at 300°C , which would suggest the presence of some unreacted thiol groups. ^{13}C CP MAS NMR spectra of SH samples reveal further details of the functional groups present in the Au-containing materials (Fig. 5). Sample SH-DMD-Au presents an intense resonance signal at 54 ppm corresponding to the C atoms attached to the sulfonic group in the propyl chain, as it has been discussed above and in agreement with the XPS spectrum. However, the intensity of this signal in the SH-hp-Au sample is lower and the signal at 26 ppm characteristic of the mercaptopropyl group is still detected, which indicates that thiol

groups are still present in this sample, in agreement with what was concluded from TGA. A signal at 59 ppm previously assigned to the C atom attached to O in the ethoxy group in the extracted samples is observed in all the spectra, which suggests that these groups have been restored due to the treatment of the samples with the ethanolic solution of the Au-containing rosemary oil in the presence of the sulfonic groups. In the spectrum of the SOc-hp-Au sample, four additional resonance signals are detected at 12.4 ppm, 22.8 ppm, 29.6 ppm and 32.5 ppm, assigned [31] to the C atoms of the octyl chain indicated in Fig. 7. The ^{29}Si MAS NMR spectrum of this sample (Fig. 7) shows the presence of two signals at -65 and -54.7 ppm, being the former more intense than the latter. They are attributed respectively to T^3 and T^2 sites, where T^m corresponds to silane species (those having C–Si bonds) in environments described as $[\text{RSi}(\text{OSi})_m(\text{OH})_{3-m}]$, $m = 1, 2$ and 3 [29]. These signals are more intense than those of the SH samples (Fig. 7), while its sulphur content is only slightly lower, which clearly evidences the presence of Si-C8 units at the channel surface.

To summarize, the immobilization of gold produces the oxidation of the S-bearing functional groups initially present in the materials to sulfonic acid, although minor amounts of thiol groups might still be present in some of the samples that were not pre-oxidized or they were so with hydrogen peroxide prior gold immobilization. This information is relevant for a proper understanding of the catalytic activity of these materials, as it will be discussed below.

Fig. 8 collects the UV-vis spectra of the Au-containing materials. In general, two bands of low intensity are observed at ~ 250 nm and ~ 300 nm, although they are hardly observed in some of them. The latter band is in the 300–450 nm range reported for 0.8 nm gold clusters stabilized with thiol groups [32], while UV bands at ~ 250 nm have been assigned to gold clusters having a partial positive charge [33]. However, it has to be considered that SPr-hp support also presents a band of weak intensity at ~ 250 nm, which could eventually be due to minor amounts of organic species adsorbed during gold deposition and still retained after washing. Nevertheless, the surface plasmon resonance band at 520 nm characteristic of Au nanoparticles is not detected, save for sample SPr-hp-Au, where a band of very weak intensity is found at this wavenumber. This sample is the one with the highest gold content, although it is still low, 1.17 wt.%, and very similar to the 1.09 wt.% of sample SH-Au, where no plasmon band is detected. Moreover, it has not been detected either in conventional SBA-15 samples with 3.5 wt.% of sulphur and 2.57 wt.% of Au prepared by the same procedure described here [8]. It is then possible that the alkyl groups present in the SPr material facilitate some agglomeration of gold species during the immobilization process. As no AuNPs are detected in

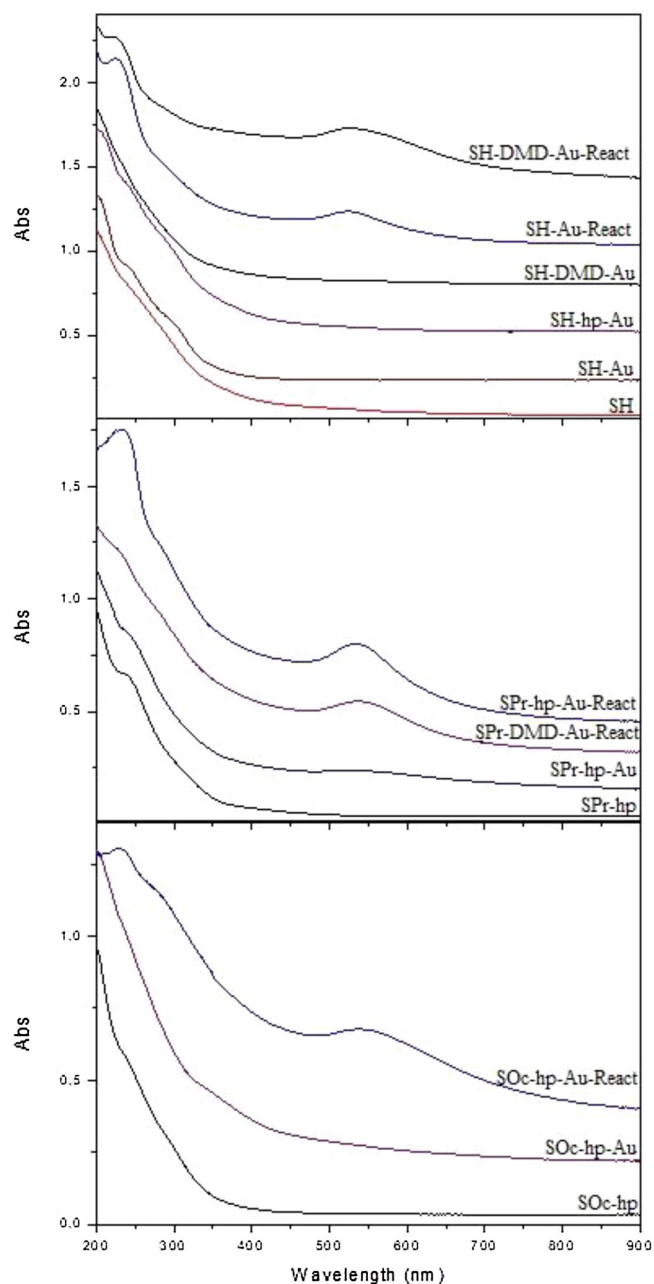


Fig. 8. UV-vis spectra of Au-containing materials before and after (samples labeled as -React) reaction.

the SOc samples, containing octyl groups and very low amount of gold, this suggests that the metal aggregation could be regulated by the density of sulfonic acid groups and their interaction with the gold species, the content of metal and the eventual presence of hydrophobic groups that would interact only weakly with the immobilized gold entities.

XPS spectra of the Au 4f spectra of SH-Au and SH-DMD-Au provide additional clues on the nature of the gold species present in these materials (Fig. 9). Two broad and symmetrical signals of Au $4f_{7/2}$ and Au $4f_{5/2}$ are detected, respectively, at BE energies of 84.5 eV and 88.1 eV for sample SH-Au, and at 0.1 eV higher BE for SH-DMD-Au. There is no evidence of more than one oxidation state of Au. The BE of these signals is about +0.5 eV higher than that commonly found for Au(0), which is 83.9 ± 0.1 eV for Au $4f_{7/2}$ [24], but it is also far from the band at 84.9 eV reported for Au(I) in a gold octanethiol complex [34]. Moreover, a BE of 83.8 eV has been reported for the Au $4f_{7/2}$ core-level of Au

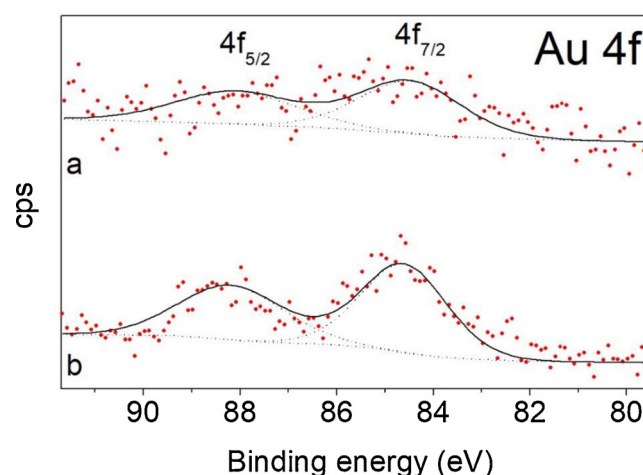


Fig. 9. Au 4f core-level spectra of samples (a) SH-Au and (b) SH-DMD-Au. Scatter points correspond to raw data and lines to curve-fitting results.

nanoparticles in the size range of 1–3 nm linked to dodecanethiol [7]. A shift of the core-level energy of Au clusters has been reported as a function of the Au nanocluster size, in such a way that the XPS BE as well as peak width have been found to increase with decreasing cluster size [24,35,36]. Therefore, the BE found here for these two Au-bearing materials would be consistent with the presence of small gold nanoclusters, but no AuNPs, in agreement with the UV-vis spectra. However, the presence of some Au(I) species at the cluster surface that would interact with the $-\text{SO}_3^-$ groups cannot be excluded.

3.4. Catalytic activity

The Au-samples were used as catalysts for the oxidation of cyclohexene in liquid phase by using molecular oxygen as oxidant. Fig. 10 depicts the conversion of cyclohexene versus reaction time for the SH catalysts (left) and alkyl-functionalized SPr and SOc materials (right). The activity of sample SH prior gold deposition has also been included for comparison purposes. It can be noticed that the activity of sample SH-Au approaches 40% at 24 h reaction, and keeps increasing up to 60% at 48 h. This behavior is in agreement with the presence of sulfonic acid groups, as it has been reported that Au-SBA-15 materials functionalized with thiol groups are inactive for this reaction under the conditions here described [8]. As the Au content of the several samples is different, it would be convenient to use the turnover number (TON, defined as the number of moles of cyclohexene converted per mole of Au) for comparison purposes, which are collected in Table 5 for 24 h of reaction. TON of SH-Au catalyst is nearly three times that of Au immobilized over rod-shape SBA-15 containing sulfonic groups prepared by the same two-liquid phases procedure describe here [8], which evidences the benefits of using the short-channel SBA-15 material as support. It is also interesting to notice that the catalyst is still active at long reaction times, a behavior that has not been seen before [8], nor it is shared by the rest of catalysts reported here. The activity (TON) of the sample pre-oxidized with DMD is slightly higher than that of SH at 24 h, but it does not increase when keeping the reaction running for an additional 24 h period. In contrast to this beneficial DMD oxidation, pre-oxidation with H_2O_2 led to less active catalysts, although the difference in activity was small (Table 5).

The effect of pre-oxidation with DMD or H_2O_2 of the catalysts containing C3 and C8 alkyl groups varies according to the chain length (Table 5). For the former (SPr catalysts), DMD is also a preferred oxidant, but the corresponding TON values are roughly the same as those of alkyl-free SH samples. However, the TON values of C8-functionalized catalysts (SOc) are clearly higher, being again DMD the most favorable pre-oxidation agent. It was discussed above that DMD can convert

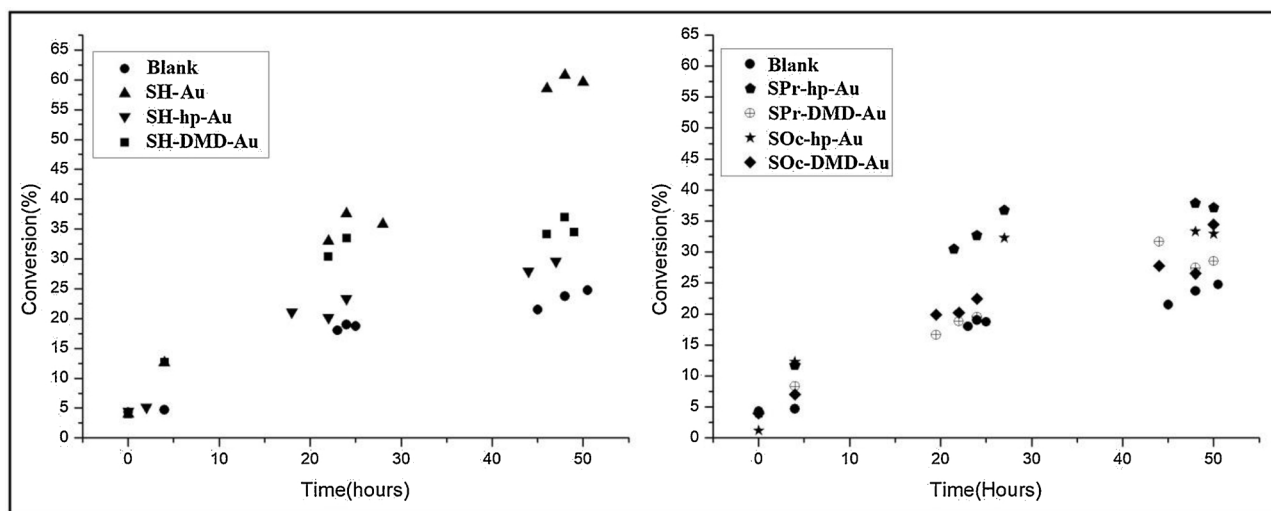


Fig. 10. Cyclohexene conversion as a function of reaction time. Left: SH catalysts. Right: SPR and SOc catalysts.

Table 5

TON ($\times 10^3$) values at 24 h. Catalyst L1-8 reported in [8] has been included for comparison.

SH-Au	SH-hp-Au	SH-DMD-Au	SPR-hp-Au	SPR-DMD-Au	SOc-hp-Au	SOc-DMD-Au	L1-8 (Ref. [8])
6.5	5.4	7.3	5.4	6.8	8.9	18.9	2.3

quantitatively the thiol groups to $-\text{SO}_3^-$, and this would explain the higher TON of the supports pre-oxidized with this reagent for each series of supports, SH, SPR and SOc. In this last case, the TON value increases by 2.5 times as compared with that of SH-DMD-Au catalyst. This effect could be most probably attributed to the higher hydrophobicity of this material, in agreement with the starting hypothesis that an increase in hydrophobicity would increase the overall activity by enhancing the adsorption of the hydrophobic cyclohexene. On the other hand, these results also evidence the relevance of the adsorption/diffusion characteristics of the porous support on the performance of the Au-catalysts.

It has been observed that the color of the catalysts evolves in the reaction medium, being purple colored at the end. Indeed, UV-vis spectra of the used catalysts show for all of them the presence of the characteristic surface plasmon resonance band at ~ 525 nm (Fig. 8), and the presence of AuNPs has been further confirmed by TEM in the case of sample SH-DMD-Au (Fig. 11). This gradual aggregation process of the gold clusters initially present in the catalysts that takes place in the course of the aerobic oxidation of cyclohexene has already been observed previously by us [8] and reported also for triphenylphosphine-stabilized Au clusters deposited on SiO_2 . In the last case, the catalytic activity has been linked to the formation of metallic particles larger than 2 nm [37]. It is also remarkable on this regard that, save for SOc samples, the TON of the different catalysts are relatively close to each other, which would mean that, in spite of the transient nature of the metal entities present in the reaction medium, they should be quite similar for all catalysts.

Selectivity to the five different products identified in this reaction is depicted in Fig. 12 as a function of total conversion for all catalysts. It can be seen that allylic oxidation to produce 2-cyclohexen-1-one, 2-cyclohexen-1-ol and 2-cyclohexenyl hydroperoxide is the preferred reaction pathway, which accounts for nearly 90% of the total products. At low conversion ($\sim 5\%$) the enol is the major product, but its selectivity decreases rapidly with conversion and it stabilizes around 20% for conversion $> \sim 15\%$. At this conversion, the selectivity to hydroperoxide reaches a maximum of $\sim 40\%$ and decreases rapidly beyond this

point. The selectivity to enone increases continuously and it becomes the dominant product for conversion $> \sim 20\%$. The complex evolution pattern of the several reaction products as a function of conversion suggests a complex reaction network, where the enol seems to be a primary product, while the hydroperoxide is a reaction intermediate that leads to the enone and enol.

4. Conclusions

SBA-15 materials functionalized with mercaptopropyl and alkyl hydrocarbon groups possessing short channels in the length range of 200–400 nm can be conveniently prepared by using P104 tri-block copolymer surfactant and appropriate synthesis conditions. The thiol groups can be efficiently pre-oxidized with dimethyldioxirane (DMD) to produce sulfonic groups, but the oxidation with hydrogen peroxide is less efficient. The simultaneous presence of octyl groups prevents to a large extent the effect of H_2O_2 on the thiol groups, although it does not affect the activity of the stronger oxidant DMD. Both pre-oxidized as well as pristine SH-bearing samples are able to immobilize gold nanoclusters synthesized by a two liquid-phases method involving the use of rosemary essential oil as organic phase and a solution of gold in *aqua regia* as aqueous phase. In addition, the immobilization process produces the partial oxidation of S-functional groups to sulfonic groups. The presence of alkyl groups decreases the amount of gold immobilized on the catalysts. No AuNPs are in general detected, the metal being present as small clusters, save in one sample where they coexist with a small amount of AuNPs. The activity of these materials in the oxidation of cyclohexene is regulated mainly by the gold content, but their average activity is much larger than that found previously for Au-catalysts prepared by the same method reported here but supported on conventional rod-shape SBA-15 possessing long channels, which evidences the benefits of reducing the diffusion pathway through the pore system. Pre-oxidation of the samples with DMD improves the turnover number (TON), an effect that has been attributed to the presence of sulfonic groups in the catalysts. Moreover, it has been found that the presence of hydrophobic octyl groups also increases notably the TON values. It has been observed for all catalysts that the gold clusters evolve in the reaction medium to form gold nanoparticles. This work evidences the influence of factors affecting the catalytic activity not directly related to the metal active phase in the course of the cyclohexene oxidation in liquid phase, in particular the chemical composition, morphology and pore length of the host support.

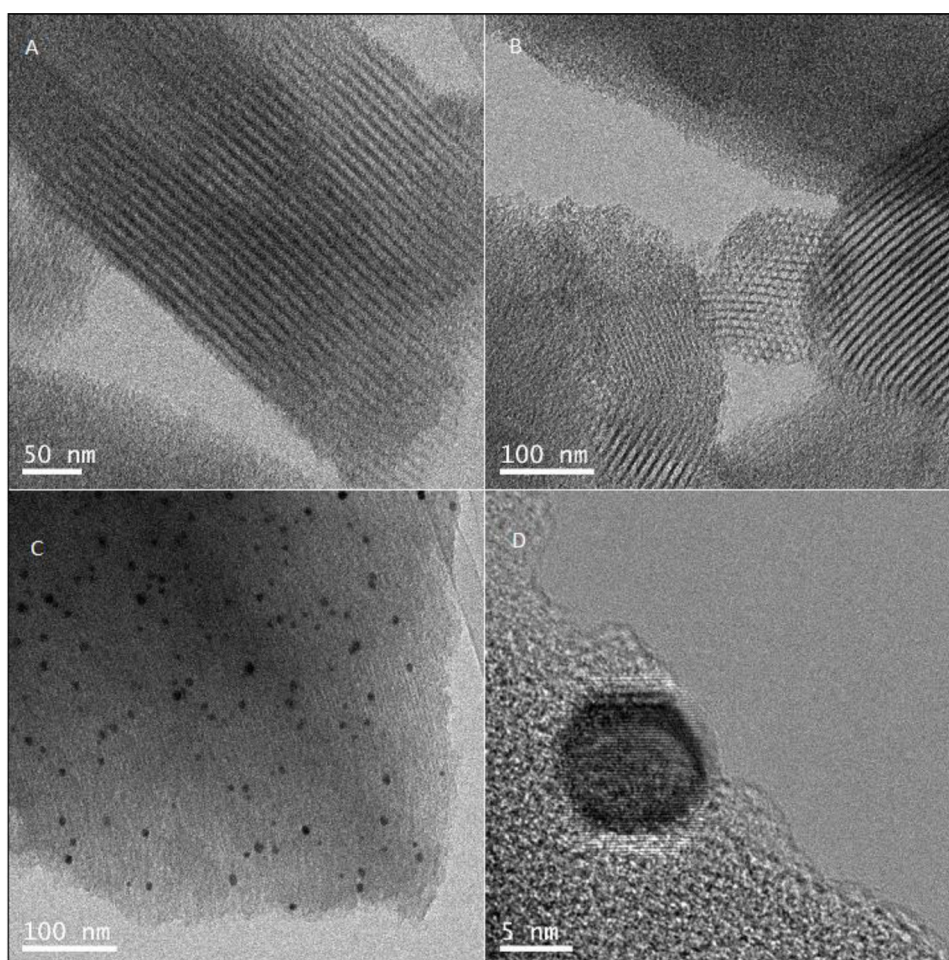


Fig. 11. TEM images of catalysts SH-DMD-Au before (top) and after (below) reaction.

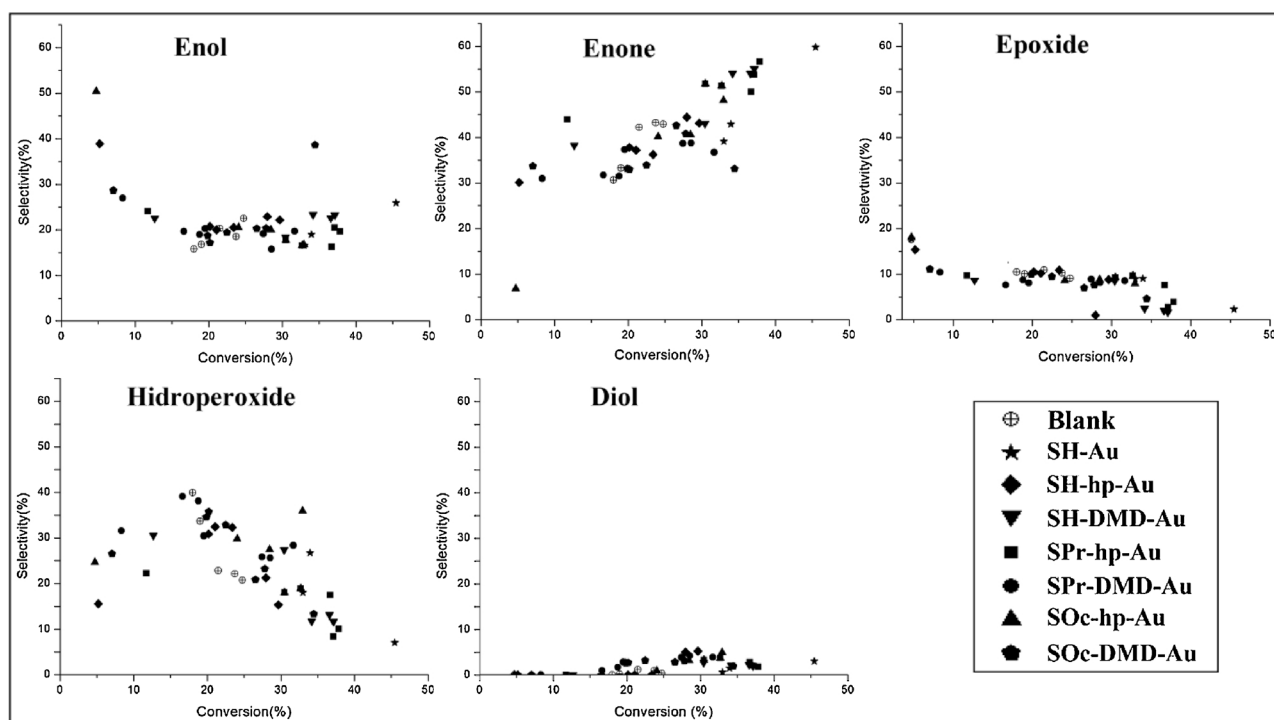


Fig. 12. Selectivity vs conversion for the five reaction products.

Acknowledgements

The authors acknowledge the current Spanish Ministry of Science, Innovation and Universities (formerly the Ministry of Economy and Competitiveness) for the funding of this study through project MAT2016-77496-R. The help of Dr. Isabel Díaz with the TEM study is greatly appreciated.

Appendix A. Supplementary data

Supplementary data associated with this article can be found, in the online version, at <https://doi.org/10.1016/j.cattod.2019.09.014>.

References

- [1] A.S.K. Hashmi, G.J. Hutchings, *Angew. Chem. Int. Ed.* 45 (2006) 7896–7963.
- [2] A. Corma, A. Leyva-Perez, M.J. Sabater, *Chem. Rev.* 111 (2011) 1657–1712.
- [3] A. Corma, H. García, *Chem. Soc. Rev.* 37 (2008) 2096–2126.
- [4] A. Mayoral, J. Agúndez, I.M. Pascual-Valderrama, J. Pérez-Pariente, *Gold Bull.* 47 (2014) 161–165.
- [5] N. Lemery, *Cours de Chymie*, L.-C. d'Houry, Paris, 1757.
- [6] M. Faraday, *Philos. Trans. R. Soc. Lond.* 147 (1857) 145–181.
- [7] M. Brust, M. Walker, D. Bethell, D.J. Schiffrin, R. Whyman, *J. Chem. Soc. Chem. Commun.* (1994) 801–802.
- [8] J. Agúndez, L. Martin, A. Mayoral, J. Pérez-Pariente, *Cat. Today* 304 (2018) 172–180.
- [9] L.-F. Gutiérrez, S. Hamoudi, K. Belkacemi, *Catalysts* 1 (2011) 97–154.
- [10] R.G. Nuzzo, D.L. Allaro, *J. Am. Chem. Soc.* 105 (1983) 4481–4483.
- [11] J.L. Love, L.A. Estroff, J.K. Kriebel, R.G. Nuzzo, G.M. Whitesides, *Chem. Rev.* 105 (2005) 1103–1169.
- [12] P. Linton, J.-C. Hernandez-Garrido, P.A. Midgley, H. Wennerström, V. Alfredsson, *Phys. Chem. Chem. Phys.* 11 (2009) 10973–10982.
- [13] P. Linton, H. Wennerström, V. Alfredsson, *Phys. Chem. Chem. Phys.* 12 (2010) 3952–3958.
- [14] W.W. Van Rhijn, D.E. De Voss, B.F. Sels, W.D. Bossaert, P.A. Jacobs, *Chem. Commun.* (1998) 317–318.
- [15] I. Diaz, F. Mohino, J. Pérez-Pariente, E. Sastre, *Thermo. Acta* 413 (2004) 201–207.
- [16] D. Margolese, J.A. Melero, S.C. Christiansen, B.F. Chmelka, G.D. Stucky, *Chem. Mater.* 12 (2000) 2448–2459.
- [17] R.W. Murray, R. Jeyaraman, *J. Org. Chem.* 50 (1985) 2847–2853.
- [18] W. Adam, L. Hadjarapoglou, *Top. Curr. Chem.* 64 (1993) 45–61.
- [19] M.D. Hughes, Y.-J. Xu, P. Jenkins, P. McMorn, P. Landon, D.I. Enache, A.F. Carley, G.A. Attard, G.J. Hutchings, F. King, E.H. Stitt, P. Johnston, K. Griffin, C.J. Kiely, *Nature* 437 (2005) 1132–1135.
- [20] H. Alshammari, P.J. Miedziak, T.E. Davies, D.J. Willock, D.W. Knight, G.J. Hutchings, *Catal. Sci. Technol.* 4 (2014) 908–911.
- [21] E. Beletskiy, M.C. Kung, H.H. Kung, *Catalytic properties of gold nanoparticles*, in: C. Louis, O. Pluchery (Eds.), *Gold Nanoparticles for Physics, Chemistry and Biology*, 2nd ed., World Scientific, New Jersey, 2017, pp. 285–318.
- [22] I. Diaz, C. Márquez-Álvarez, F. Mohino, J. Pérez-Pariente, E. Sastre, *J. Catal.* 193 (2000) 283–294.
- [23] J.D. Webb, T. Seki, J.F. Goldston, M. Pruski, C.M. Crudden, *Microporous Mesoporous Mater.* 203 (2015) 123–131.
- [24] M.-C. Bourg, A. Badia, R.B. Lennox, *J. Phys. Chem. B* 104 (2000) 6562–6567.
- [25] E. Cano-Serrano, G. Blanco-Brieva, J.M. Campos-Martin, J.L.G. Fierro, *Langmuir* 19 (2003) 7621–7627.
- [26] J. Hopkins, J.Ps. Badyal, *Macromolecules* 27 (1994) 5498–5503.
- [27] M.M. Nasef, H. Saidi, *Appl. Surf. Sci.* 252 (2006) 3073–3084.
- [28] G. Zotti, S. Zecchin, G. Schiavon, F. Louwet, L. Groenendaal, X. Crispin, W. Osikowicz, W. Salaneck, M. Fahlman, *Macromolecules* 36 (2003) 3337–3344.
- [29] A.C. Cattaneo, C. Ferar, D.C. Villa, S. Angioni, C. Milanese, D. Capsoni, S. Grandi, P. Mustarelli, V. Allodi, G. Mariotto, S. Brutti, E. Quatarone, *Microporous Mesoporous Mater.* 219 (2016) 210–220.
- [30] P. Wu, P. Bai, Z. Lei, K.P. Loh, X.S. Zhao, *Microporous Mesoporous Mater.* 141 (2011) 222–230.
- [31] S. Dirè, V. Tagliuzucca, E. Callone, A. Quarante, *Mat. Chem. Phys.* 126 (2011) 909–917.
- [32] G.H. Woehle, M.G. Warner, J.E. Hutchinson, *J. Phys. Chem. B* 106 (2002) 9979–9981.
- [33] N. Bogdanchikova, A. Pestrjakov, I. Tuzovskaya, T.A. Zepeda, M.H. Farias, H. Tiznado, O.A. Martyniuk, *Fuel* 110 (2013) 40–47.
- [34] A. McNeille, D.H. Brown, W.E. Smith, M. Gibson, L. Watson, *J. Chem. Soc. Dalton Trans.* (1980) 767–770.
- [35] S. Peters, S. Peredkov, M. Neeb, W. Eberhardt, M. Al-Hada, *Surf. Sci.* 608 (2013) 129–134.
- [36] A.A. Tal, W. Olovsson, I.A. Abrikosov, *Phys. Rev. B* 95 (2017) article number 245402.
- [37] B.G. Donoeva, D.S. Ovoshchnikov, V.B. Golovko, *ACS Catal.* 3 (2013) 2986–2991.